Computational Study on the Mechanism and Rate Constant for the $C_6H_5 + C_6H_5NO$ Reaction

Z. F. Xu and M. C. Lin*

Department of Chemistry, Emory University, Atlanta, Georgia 30322

Received: April 28, 2005; In Final Form: July 31, 2005

The reaction mechanism of $C_6H_5 + C_6H_5NO$ involving four product channels on the doublet-state potential energy surface has been studied at the B3LYP/6-31+G(d, p) level of theory. The first reaction channel occurs by barrierless association forming $(C_6H_5)_2NO$ (biphenyl nitroxide), which can undergo isomerization and decomposition. The second channel takes place by substitution reaction producing $C_{12}H_{10}$ (biphenyl) and NO. The third and fourth channels involve direct hydrogen abstraction reactions producing $C_6H_4NO + C_6H_6$ and $C_6H_5NOH + C_6H_4$, respectively. Bimolecular rate constants of the above four product channels have been calculated in the temperature range 300−2000 K by the microcanonical Rice−Ramsperger−Kassel−Marcus theory and/or variational transition-state theory. The result shows the dominant reactions are channel 1 at lower temperatures ($T < 800$ K) and channel 3 at higher temperatures ($T > 800$ K). The total rate constant at 7 Torr He is predicted to be $k_t = 3.94 \times 10^{21}\ T^{-3.09} \exp(-699/T)$ for 300−500 K, $2.09 \times 10^{20}\ T^{-3.56} \exp(2315/T)$ for 500−1000 K, and $1.51 \times 10^{2}\ T^{3.30} \exp(-3043/T)$ for 1000−2000 K (in units of $cm^3\ mol^{-1}\ s^{-1}$), agreeing reasonably with the experimental data within their reported errors. The heats of formation of key products including biphenyl nitroxide, hydroxyl phenyl amino radical, and *N*-hydroxyl carbazole have been estimated.

Introduction

C_6H_5NO (nitrosobenzene) is one of the most convenient sources of phenyl radical for its kinetic studies. Over the years, we have employed it in our studies of C_6H_5 reactions in a shock tube,[1] in a Saalfeld reactor[2] using laser photolysis/mass spectrometry,[3−5] in a static reactor by FTIR spectrometry,[4−6] and in a series of experiments by cavity ringdown spectrometry.[7−10]

In 1997, Park and Lin[3] measured the rate constant for the recombination of C_6H_5 radicals, generated by the photolysis of C_6H_5NO, by using a laser photolysis/mass spectrometric technique at around 7 Torr helium pressure in the temperature range 300−500 K. They detected the occurrence of the $C_6H_5 + C_6H_5NO$ reaction by mass balance and evaluated the rate constant for the association reaction, $k = 4.9 \times 10^{12} \exp(+34/T)$ $cm^3/(mol{\cdot}s)$ in the temperature range. The magnitude of the rate constant for $C_6H_5 + C_6H_5NO$ compares reasonably with those for the analogous alkyl radical reactions.[11,12] Aside from this experimental study for the association reaction, no other experimental or theoretical investigation has been made to date.

The mechanism for the title reaction, similar to those of alkyl counterparts, is not well-established, particularly under high-temperature combustion conditions. The goal of the present study lies in the characterization of the various isomerization/fragmentation processes involving internally excited association product, $(C_6H_5)_2NO$, employing the hybrid density functional theory (DFT) in conjunction with the multichannel (RRKM) theory. The result is discussed in the following sections in detail.

* Corresponding author e-mail: chemmcl@emory.edu.

Computational Methods

The geometries of the reactants, products, intermediates, and transition states on the ground electronic doublet-state potential energy surface (PES) of the $C_6H_5 + C_6H_5NO$ system were optimized[13] by the DFT at the B3LYP level[14,15] with the basis set 6-31+G(d, p). All the stationary points have been identified for local minima and transition state by vibrational analysis. Unscaled vibrational frequencies were employed for the calculation of zero-point energy (ZPE) corrections, the characterization of stationary points, and rate constant calculations. On account of the large size of this system, improvement of the energies with a high level theory is not realistic at present. All electronic structure calculations were performed with Gaussian 98 program.[16]

The microcanonical Rice−Ramsperger−Kassel−Marcus (RRKM) theory[17] was employed to calculate the rate constants for the barrierless association reaction producing $(C_6H_5)_2NO$ and its fragments by the VARIFLEX code.[18] The component rates were evaluated at the E/J-resolved level, and the pressure dependence was treated by one-dimensional master equation calculations using the Boltzmann probability of the complex for the J-distribution. In addition, the minimum potential energy path (MEP) of the barrierless association process was represented by the Morse function, $V(R) = D_e\{1 - \exp[-\beta(R - R_e)]\}^2$. Here, D_e is the bonding energy excluding zero-point vibrational energy for an association reaction, R is the reaction coordinate (i.e., the distance between the two bonding atoms), and R_e is the equilibrium value of R at the stable intermediate structure.

The rate constants for simple exchange reactions with distinct transition states were calculated with variational or conventional transition state theory with Eckart tunneling corrections.

10.1021/jp0522157 CCC: $30.25
Published on Web 09/16/2005

Results and Discussion

Potential Energy Surface and Reaction Mechanism. On the ground-state PES, four reaction channels were investigated as follows:

$$C_6H_5NO + C_6H_5 \rightarrow$$

$$(C_6H_5)_2NO \rightarrow \text{isomerization/disassociation} \quad (1)$$

$$\rightarrow C_6H_5{-}C_6H_5 + NO \quad (2)$$

$$\rightarrow C_6H_4NO + C_6H_6 \quad (3)$$

$$\rightarrow C_6H_5NOH + C_6H_4 \quad (4)$$

The geometries of the reactants, products, intermediates, and transition states optimized at the B3LYP/6-31+G(d, p) level of theory are shown in Figure 1. The predicted vibrational frequencies and moments of inertia for all of these species are summarized in Table 1. The potential energy diagram obtained at the B3LYP/6-31+G(d, p) level of theory is presented in Figure 2.

Channel 1 includes a serial of complicated association/isomerization/disassociation processes; the most stable intermediate, $(C_6H_5)_2NO$, in this channel is formed barrierlessly from the reactants. The exothermicity was predicted to be 58.4 kcal/mol at the B3LYP/6-31+G(d, p) level of theory. There are two branching processes from $(C_6H_5)_2NO$: one is a direct elimination of the oxygen atom with no intrinsic barrier to form $(C_6H_5)_2N + O$, and the other is the isomerization with one of the two hydrogen atoms closest to the O atom, migrating from C to O to form the radical, $C_6H_5N(OH)C_6H_4$ (LM1), via the transition state TS1. Comparing the energy changes in these two processes, we can assert that the latter is more favorable than the former because TS1 lies below $(C_6H_5)_2N + O$ by 23.9 kcal/mol at the B3LYP/6-31+G(d, p) level of theory. Although the isomerization barrier, 51.2 kcal/mol, is quite high, it can proceed readily since the TS1 and LM1 are −7.2 and −10.7 kcal/mol lower than the reactants, respectively. LM1 can further undergo reactions by three paths. The first path, which is energetically most favored, takes place via TSiso, LM1iso, TS2, LM2, and TS3 to form products P1 (*N*-hydroxyl carbazole) + H. TSiso is a rotation transition state only higher than LM1 by 1.0 kcal/mol, and LM1iso is an isomer of LM1 with the energy of 1.1 kcal/mol lower than LM1. Transition states TS2 and TS3 lead to the carbon−carbon bond forming and the hydrogen atom eliminating processes, respectively; their energies relative to that of the reactants are −2.9 and −10.9 kcal/mol, respectively. Since the products P1 + H are 17.3 kcal/mol lower than the reactants, this sub-channel would be the most favored lower-energy process. The second path produces P2 ($C_{12}H_9N$) + OH by OH elimination from LM1 via the transition state TS4. P2 is a highly energetic isomer of carbazole that can in principle dissociate into C_6H_5N and *o*-C_6H_4 fragments (see Figure 1). The third path occurs by the hydrogen-atom migrating from O to the C atom to which the N atom attached via the transition state TS5 followed by the C−N bond breaking via the intermediate LM3 and transition state TS6 to form the products $C_6H_4NO + C_6H_6$. According to Figure 2, the latter two paths have high barriers at TS4 and TS5 (54.5 and 71.0 kcal/mol, respectively) above the reactants; they are highly unlikely to occur.

Channel 2 is an NO-displacement process that involves the attack of C_6H_5 on the carbon atom connecting the NO group in C_6H_5NO along with the concurrent breaking C−N bond of C_6H_5NO. In the transition state (TS7) of this channel, the C−C forming and C−N breaking bonds are 2.227 and 1.469 Å, respectively, and both planes of phenyls are nearly vertical to each other as seen in Figure 1. This reaction channel is predicted to have a potential barrier of 9.0 kcal/mol and is a highly exothermic process with the products $C_6H_5{-}C_6H_5 + NO$ lying below the reactants by 56.0 kcal/mol.

Channel 3 contains five direct hydrogen abstraction reactions since each of the five different hydrogen atoms of C_6H_5NO

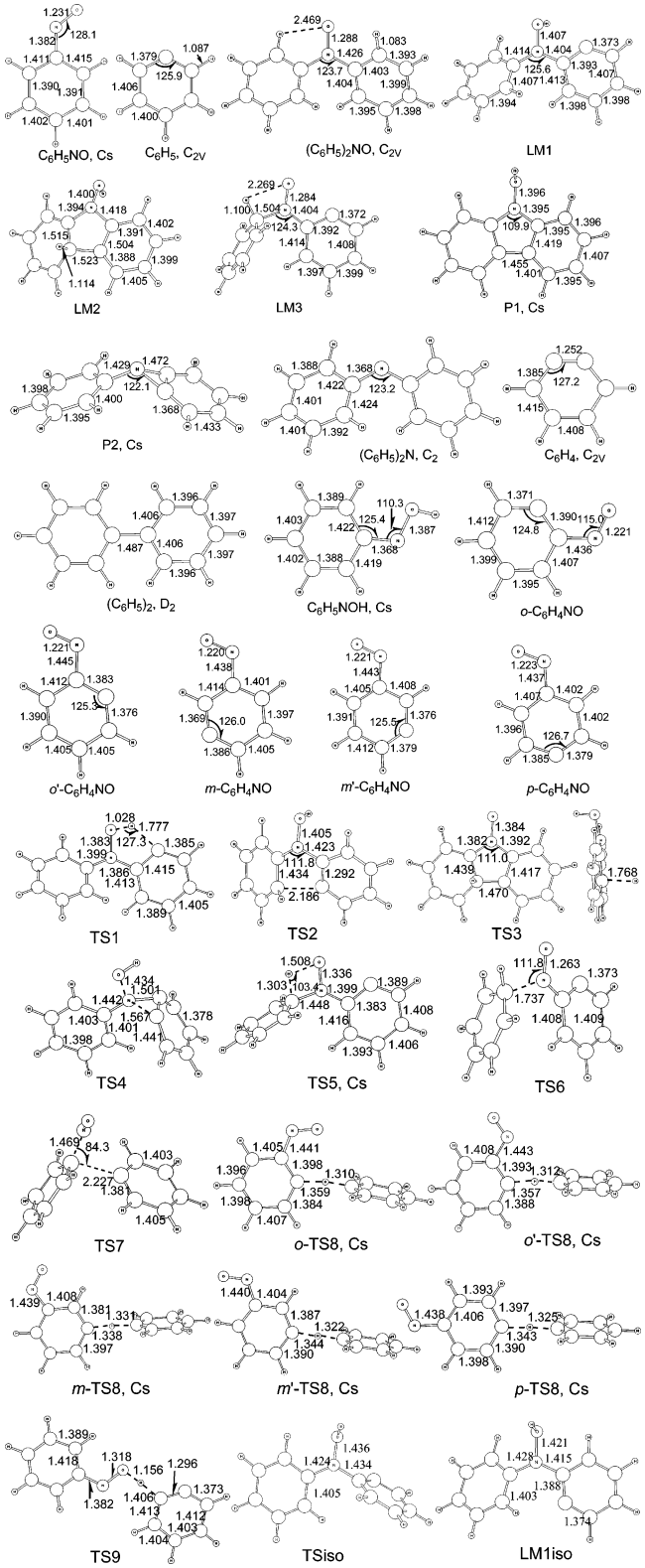

Figure 1. Geometries of the reactants, products, intermediates, and transition states (length in Å and angle in °) optimized at the B3LYP/6-31+G(d, p) level of theory.

TABLE 1: Rotational Moments of Inertia and Harmonic Frequencies of All Species Calculated at the B3LYP/6-31+G(d, p) Level of Theory

species	I_a, I_b, I_c (amu)	frequenies (cm^{-1})
C_6H_5NO	344.6, 1103.6, 1448.3	114, 248, 257, 419, 449, 472, 623, 680, 684, 773, 834, 861, 958, 997, 1015, 1015, 1039, 1103, 1139, 1191, 1206, 1343, 1375, 1491, 1509, 1584, 1641, 1654, 3187, 3198, 3206, 3215, 3223
C_6H_5	288.2, 323.0, 611.3	399, 424, 597, 616, 661, 718, 812, 892, 964, 981, 990, 1016, 1052, 1074, 1177, 1177, 1308, 1338, 1464, 1475, 1579, 1634, 3173, 3180, 3193, 3195, 3204
$(C_6H_5)_2NO$	1050.1, 4303.9, 5028.3	37, 64, 98, 131, 232, 243, 306, 374, 415, 423, 425, 462, 542, 578, 627, 628, 643, 697, 700, 737, 766, 774, 843, 851, 919, 930, 940, 981, 985, 999, 999, 1010, 1011, 1046, 1048, 1104, 1107, 1156, 1182, 1183, 1192, 1205, 1279, 1333, 1340, 1359, 1362, 1395, 1485, 1498, 1517, 1518, 1624, 1632, 1632, 1638, 3185, 3185, 3194, 3194, 3207, 3208, 3219, 3222, 3233, 3233
LM1	1060.1, 4336.0, 5084.7	25, 46, 93, 120, 214, 225, 288, 333, 347, 395, 408, 420, 472, 518, 563, 614, 627, 629, 671, 705, 726, 741, 765, 832, 845, 909, 928, 929, 973, 975, 979, 995, 1010, 1034, 1049, 1063, 1110, 1130, 1179, 1183, 1199, 1234, 1274, 1320, 1342, 1361, 1362, 1407, 1461, 1477, 1490, 1529, 1571, 1628, 1638, 1649, 3180, 3182, 3189, 3190, 3202, 3205, 3211, 3215, 3227, 3646
LM2	1323.5, 3037.5, 4228.4	82, 115, 135, 194, 225, 295, 333, 358, 396, 436, 461, 492, 515, 539, 567, 595, 618, 653, 691, 722, 745, 752, 764, 832, 877, 881, 908, 947, 949, 956, 985, 996, 1019, 1042, 1077, 1116, 1129, 1166, 1177, 1190, 1219, 1241, 1283, 1291, 1322, 1346, 1378, 1392, 1418, 1432, 1494, 1505, 1542, 1617, 1639, 1657, 2818, 3175, 3182, 3191, 3197, 3201, 3205, 3214, 3219, 3596
LM3	1408.7, 3506.0, 4246.9	33, 48, 67, 115, 162, 202, 265, 357, 360, 391, 438, 443, 510, 522. 587, 610, 617, 630, 660, 694, 740, 744, 764, 822, 822, 915, 924, 965, 970, 975, 976, 978, 992, 1032, 1033, 1049, 1123, 1131, 1173, 1182, 1195, 1219, 1266, 1288, 1307, 1350, 1351, 1402, 1432, 1451, 1465, 1474, 1542, 1571, 1599, 1632, 2977, 3179, 3181, 3182, 3192, 3201, 3202, 3204, 3214, 3234
P1	1282.7, 3063.9, 4333.5	102, 113, 150, 213, 253, 297, 299, 360, 426, 433, 453, 530, 558, 565, 584, 625, 639, 729, 735. 750, 758, 778, 782, 862, 865, 924, 943, 943, 980, 981, 1016, 1037, 1046, 1057, 1137, 1142, 1175, 1183, 1238, 1254, 1311, 1338, 1346, 1384, 1396, 1420, 1476, 1486, 1518, 1519, 1623, 1623, 1649, 1666, 3182, 3183, 3190, 3191, 3204, 3205, 3214, 3214, 3751
P2	780.8, 3853.5, 4358.0	15, 52, 101, 170, 272, 305, 317, 413, 444, 481, 553, 585, 604, 629, 669, 696, 721, 730, 741, 767, 835, 876, 901, 907, 922, 966, 970, 977, 987, 991, 1012, 1046, 1091, 1103, 1124, 1180, 1181, 1192, 1237, 1287, 1334, 1359, 1389, 1460, 1486, 1495, 1522, 1567, 1631, 1643, 1818, 3180, 3184, 3186, 3196, 3200, 3201, 3210, 3218, 3220
$(C_6H_5)_2$	632.3, 3321.4, 3801.5	65, 94, 125, 268, 312, 367, 414, 420, 501, 556, 622, 626, 638, 709, 711, 751, 754, 793, 857, 857, 923, 939, 982, 983, 1001, 1001, 1010, 1015, 1022, 1054, 1068, 1103, 1108, 1183, 1184, 1204, 1212, 1306, 1308, 1343, 1356, 1367, 1464, 1492, 1519, 1542, 1615, 1631, 1649, 1650, 3177, 3177, 3182, 3184, 3192, 3195, 3197, 3200, 3206, 3208
C_6H_5NOH	353.7, 1135.4, 1489.2	136, 241, 257, 415, 444, 456, 534, 613. 621, 682, 768, 830, 833, 913, 980, 990, 994, 1034, 1046, 1110, 1164, 1179, 1248, 1324, 1357, 1414, 1489, 1495, 1592, 1613, 3182, 3191, 3204, 3212, 3236, 3808
o-C_6H_4NO	329.6, 1108.1, 1437.8	114, 216, 236, 415, 434, 483, 609, 661, 675, 754, 833, 861, 961, 979, 997, 1033, 1113, 1155, 1181, 1260, 1354, 1426, 1463, 1572, 1588, 1644, 3184, 3194, 3199, 3213
C_6H_4	257.7, 317.2, 574.9	393, 405, 433, 587, 619, 750, 838, 869, 922, 967, 1000, 1082, 1108, 1163, 1277, 1319, 1428, 1471, 1488, 2016, 3177, 3192, 3217, 3220
C_6H_6	317.9, 317.9, 635.8	411, 411, 619, 619, 692, 712, 864, 866, 984, 985, 1013. 1015, 1018, 1062, 1062, 1178, 1199, 1199, 1355, 1379, 1516, 1516, 1643, 1643, 3167, 3177, 3177, 3192, 3192, 3202,
OH	3.2, 3.2	3706
NO	35.7, 35.7	1980
TS1	990.3, 4394.1, 5225.9	*i*824, 42, 65, 108, 154, 221, 234, 315, 374, 404, 417, 431, 504, 527, 579, 624, 627, 663, 692, 697, 730, 751, 766, 829, 841, 858, 918, 935, 941, 978, 984, 998, 1008, 1041, 1047, 1060, 1116, 1130, 1165, 1182, 1185, 1202, 1245, 1314, 1340, 1354, 1364, 1418, 1431, 1476, 1506, 1524, 1563, 1599, 1622, 1638, 2517, 3165, 3182, 3187, 3192, 3195, 3204, 3210, 3235, 3237
TS2	1284.8, 3405.9, 4438.1	*i*349, 71, 109, 148, 191, 260, 286, 350, 380, 401, 415, 443, 503, 551, 559, 570, 606, 623, 695, 714, 730, 750, 757, 816, 853, 861, 906, 932, 938, 973, 982, 983, 1009, 1034, 1042, 1052, 1097, 1129, 1177, 1177, 1187, 1242, 1267, 1291, 1339, 1356, 1361, 1402, 1458, 1462, 1473, 1510, 1584, 1590, 1609, 1631, 3169, 3172, 3185, 3186, 3196, 3197, 3207, 3210, 3224, 3604
TS3	1301.5, 3081.8, 4333.1	*i*908, 87, 114, 145, 209, 248, 281, 292, 356, 414, 428, 435, 479, 502, 541, 557, 572, 584, 630, 642, 727, 737, 746, 755, 778, 797, 861, 869, 927, 936, 947, 975, 983, 1012, 1033, 1043, 1066, 1136, 1146, 1173, 1182, 1232, 1253, 1328, 1331, 1348, 1375, 1395, 1417, 1473, 1487, 1514, 1518, 1593, 1626, 1638, 1662, 3185, 3186, 3194, 3197, 3207, 3208, 3217, 3218, 3655
TS4	1389.9, 3181.8, 3923.8	*i*289, 37, 108, 113, 153, 214, 239, 319, 361, 368, 420, 436, 453, 510, 570, 589, 600, 627, 663, 696, 707, 761, 768, 829, 836, 854, 910, 923, 940, 957, 969, 971, 977, 994, 996, 1011, 1054, 1118, 1130, 1180, 1184, 1186, 1194, 1217, 1347, 1363, 1385, 1424, 1428, 1441, 1490, 1524, 1556, 1575, 1630, 1639, 3170, 3184, 3186, 3195, 3197, 3201, 3209, 3260, 3261, 3713

TABLE 1 (Continued)

species	I_a, I_b, I_c (amu)	frequenies (cm^{-1})
TS5	1116.8, 4361.4, 4823.3	*i*1398, 45, 66, 67, 143, 168, 188, 273, 335, 387, 388, 424, 435, 499, 561, 599, 612, 652, 660, 676, 730, 744, 781, 802, 840, 901, 937, 942, 965, 975, 983, 987, 998, 1022, 1025, 1034, 1105, 1106, 1134, 1176, 1180, 1197, 1248, 1281, 1300, 1304, 1350, 1358, 1442, 1450, 1463, 1485, 1557, 1559, 1595, 1628, 1857, 3145, 3167, 3188, 3191, 3196, 3204, 3211, 3216, 3220
TS6	1530.2, 3263.9, 3987.2	*i*467, 25, 55, 89, 142, 158, 197, 272, 356, 399, 405, 439, 462, 543, 596, 600, 611, 633, 654, 668, 719, 750, 789, 794, 845, 854, 932, 939, 974, 977, 983, 985, 1006, 1014, 1038, 1041, 1124, 1151, 1157, 1179, 1183, 1197, 1262, 1268, 1327, 1349, 1368, 1371, 1452, 1458, 1466, 1469, 1545, 1575, 1604, 1629, 3107, 3176, 3181, 3183, 3193, 3196, 3202, 3204, 3211, 3233
TS7	1633.0, 3606.8, 4019.7	*i*334, 26, 50, 97, 112, 135, 166, 251, 271, 362, 401. 422, 426, 446, 591, 607, 615, 652, 674, 679, 727, 741, 798, 826, 830, 904, 907, 964, 969, 981, 985, 994, 996, 1018, 1028, 1051, 1081, 1083, 1103, 1175, 1179, 1184, 1193, 1319, 1329, 1340, 1355, 1466, 1471, 1479, 1484, 1578, 1584, 1593, 1625, 1635, 3174, 3181, 3183, 3191, 3194, 3201, 3204, 3206, 3212, 3218
o-TS8	1296.5, 5175.1, 5830.7	*i*1544, 10, 36, 41, 85, 137, 153, 183, 245, 268, 404, 422, 437, 456, 493, 613, 614, 666, 681, 686, 688, 728, 773, 837, 840, 884, 906, 970, 971, 985, 996, 1005, 1013, 1037, 1045, 1078, 1082, 1113, 1145, 1179, 1182, 1188, 1203, 1232, 1296, 1342, 1352, 1363, 1454, 1473, 1479, 1503, 1582, 1604, 1612, 1633, 1643, 3174, 3178, 3180, 3190, 3190, 3195, 3196, 3204, 3210
o′-TS8	1414.2, 5369.4, 6142.6	*i*1526, 13, 33, 39, 106, 130, 140, 184, 237, 282, 405, 424, 432, 460, 483, 613, 613, 654, 688, 690, 702, 727, 773, 825, 838, 881, 907, 972, 975, 984, 997, 1007, 1014, 1038, 1042, 1078, 1080, 1112, 1149, 1180, 1183, 1188, 1196, 1232, 1288, 1342, 1352, 1362, 1458, 1479, 1479, 1503, 1574, 1605, 1613, 1633, 1638, 3174, 3180, 3180, 3190, 3192, 3195, 3201, 3204, 3212
m-TS8	1242.6, 6581.2, 7182.8	*i*1560, 19, 32, 39, 112, 132, 146, 190, 253, 270, 404, 421. 436, 449, 481, 611, 614, 663, 675, 690, 690, 728, 794, 841, 846, 906, 909, 945, 973, 997. 997, 999, 1010, 1022, 1047, 1077, 1078, 1100, 1137, 1180, 1181, 1188, 1221, 1231, 1311, 1341, 1350, 1364, 1448, 1478, 1485, 1502, 1569, 1606, 1615, 1632, 1642, 3174, 3179, 3182, 3188, 3193, 3197, 3203, 3204, 3212
m′-TS8	1007.6, 7198.1, 7564.6	*i*1549, 20, 33, 37, 100, 137, 161, 190, 246, 264, 404, 419, 435, 448, 489, 611, 614, 656, 674, 690, 710, 729, 797, 838, 842, 904, 910, 946, 974, 997, 1000, 1002, 1010, 1021, 1048, 1074, 1078, 1106, 1134, 1180, 1186, 1189, 1215, 1228, 1310, 1342, 1350, 1365, 1452, 1476, 1478, 1502, 1576, 1602, 1610, 1632, 1644, 3174, 3179. 3180, 3189, 3194, 3194, 3195, 3204, 3221
p-TS8	683.6, 8035.7, 8078.2	*i*1556, 22, 29, 34, 95, 142, 149, 179, 267, 278, 404, 411, 436, 471, 472, 613, 620, 639, 689, 690, 698, 729, 822, 831, 841, 845, 910, 974, 977, 987, 991, 1000, 1013, 1027, 1046, 1078, 1093, 1105, 1134, 1180, 1188, 1191, 1213, 1230, 1320, 1342, 1350, 1365, 1431, 1478, 1487, 1502, 1562, 1608, 1624, 1632, 1634, 3174, 3180, 3186, 3189, 3189, 3194, 3204, 3204, 3213
TS9	753.5, 7688.0, 8170.2	*i*2055, 18, 29, 33, 97, 106, 166, 202, 271, 359, 399, 418, 446, 468, 498, 569, 599, 621, 622, 681, 689, 733, 769, 841, 846, 853, 862, 924, 927, 974, 984, 998, 999, 1015, 1035, 1050, 1102, 1109, 1129, 1161, 1168, 1180, 1218, 1243, 1293, 1326, 1337, 1363, 1402, 1479, 1491, 1492, 1500, 1520, 1603, 1620, 1787, 3176, 3183, 3192, 3192, 3204, 3211, 3213, 3223, 3233
TSiso	1149.3, 4241.9, 4770.3	*i*12, 38, 73, 137, 214, 234, 306, 335, 349, 417, 421, 454, 466, 550, 571, 614, 625, 629, 699, 706, 725, 755, 764, 838, 854, 904, 914, 948, 974, 980, 987, 991, 994, 1007, 1041, 1053, 1113, 1118, 1173, 1182, 1200, 1214, 1256, 1289, 1336, 1339, 1360, 1364, 1448, 1468, 1489, 1525, 1581, 1628, 1631, 1647, 3179, 3180, 3187, 3188, 3195, 3205, 3207, 3220, 3240, 3786
LM1iso	1154.0, 4099.7, 4911.0	149, 214, 242, 301, 361, 366, 407, 418, 421, 481, 536, 560, 615, 621, 628, 673, 705, 724, 741, 768, 833, 845, 909, 921, 924, 973, 975, 980, 996, 1011, 1024, 1046, 1051, 1105, 1128, 1175, 1182, 1195, 1230, 1250, 1311, 1341, 1345, 1358, 1379, 1456, 1474, 1489, 1525, 1572, 1630, 1639, 1648, 3179, 3181, 3188, 3190, 3202, 3204, 3214, 3221, 3234, 3776

(arising from the orientation of the NO group on the plane of the C_6H_5 ring) can be abstracted by C_6H_5 to form C_6H_6 and five different C_6H_4NO radicals. In the corresponding five transition states (*o*-TS8, *o*′-TS8, *m*-TS8, *m*′-TS8, and *p*-TS8), the C−H breaking bond distances are 1.359, 1.357, 1.338, 1.344, and 1.343 Å, while the other C−H forming bond distances are 1.310, 1.312, 1.331, 1.322, and 1.325 Å, respectively. The potential barriers of the hydrogen abstraction reactions via these transition states are 9.5, 8.6, 7.2, 7.6, and 7.5 kcal/mol higher than the reactants, respectively. Apparently, these hydrogen abstraction reactions take place more readily on the meta and para sites than on the ortho sites because of the steric effect of the NO group at the ortho positions.

Channel 4 is another direct hydrogen abstraction reaction producing C_6H_5NOH and C_6H_4. The transition state (TS9) of this channel shows the transfer of one of the hydrogen atoms ortho to the radical center of C_6H_5 to the oxygen of C_6H_5NO. The forming O−H bond and the breaking C−H bond are 1.156 and 1.406 Å, respectively. The potential barrier of this reaction channel is predicted to be 29.9 kcal/mol, and its heat of reaction is 26.7 kcal/mol. Comparing it with channel 3, this reaction channel cannot compete effectively.

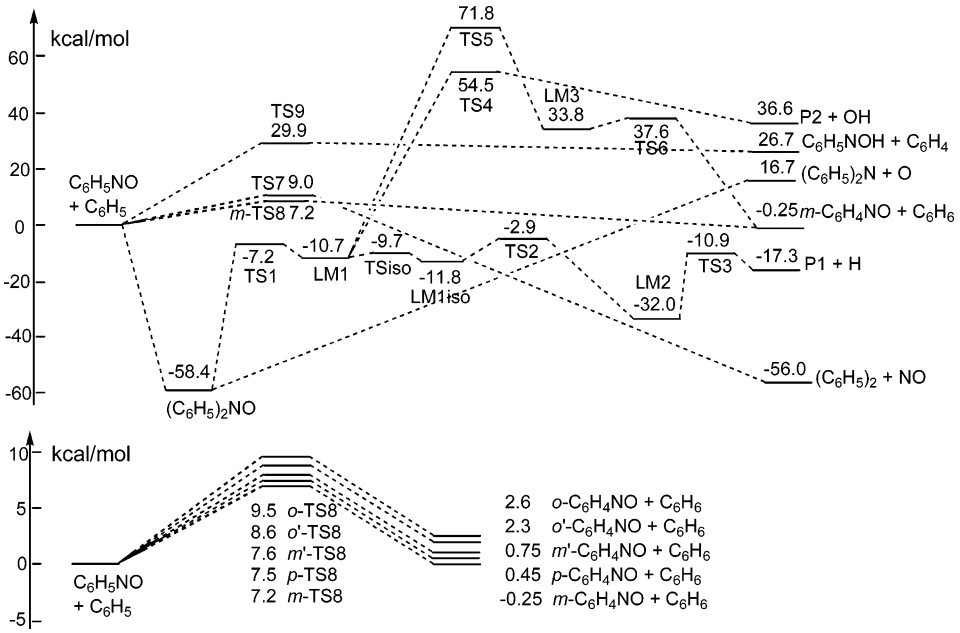

Figure 2. Schematic energy diagram predicted at the B3LYP/6-31+G(d, p) level of theory on the doublet-state potential energy surface.

TABLE 2: Heats of Reaction and Formation of Some Species (in kcal/mol) Predicted at the B3LYP/6-31+G(d, p) Level of Theory

species	reaction[a]	$\Delta_r H_0^\circ$	$\Delta_f H_0^\circ$
C_6H_5NOH	$C_6H_5 + C_6H_5NO \rightarrow C_6H_5NOH + C_6H_4$	26.7	53
$(C_6H_5)_2NO$	$C_6H_5 + C_6H_5NO \rightarrow (C_6H_5)_2NO$	−58.4	77
	$C_6H_5CO + C_6H_5NO \rightarrow (C_6H_5)_2NO + CO$	−31.8	79
P1	$C_6H_5 + C_6H_5NO \rightarrow P1 + H$	−17.3	66
P2	$C_6H_5 + C_6H_5NO \rightarrow P2 + OH$	36.6	163

[a] The heats of formation from literature: $\Delta_f H_0^\circ(C_6H_5) = 84.3 \pm 0.6$ kcal/mol (ref 19), $\Delta_f H_0^\circ(C_6H_5NO) = 51.0 \pm 0.8$ kcal/mol (ref 20), $\Delta_f H_0^\circ(C_6H_4) = 108.7 \pm 3.0$ kcal/mol (ref 21), $\Delta_f H_0^\circ(C_6H_5CO) = 32.5 \pm 1.5$ kcal/mol (ref 22), $\Delta_f H_0^\circ(CO) = -27.2 \pm 0.1$ kcal/mol (ref 23), $\Delta_f H_0^\circ(H) = 51.6$ kcal/mol (ref 23), $\Delta_f H_0^\circ(OH) = 8.8 \pm 0.1$ kcal/mol (ref 24).

In addition, based on the heats of reactions predicted at the B3LYP/6-31+G(d, p) level of theory and the known heats of formation of the species involved, the heats of formation of four products (biphenyl nitroxide, *N*-hydroxyl carbazole (P1), $C_{12}H_9N$ (P2, an isomer of carbazole), and hydroxyl phenyl amino radical (C_6H_5NOH)) have been estimated, as shown in Table 2. Among these four products, only the heat of formation of C_6H_5NOH has been reported to be 51 ± 1 kcal/mol.[20] This value is in reasonable agreement with the present result, 53 ± 5 kcal/mol, which convolutes all estimated errors as given in the footnote of Table 2.

From the above discussion on the PES of the C_6H_5 + C_6H_5NO system, it can be seen that the lowest energy channel is the formation of *N*-hydroxyl carbazole (P1) + H through the intermediates $(C_6H_5)_2NO$, LM1, and LM2. The maximum energy among three transition states of this process is 2.9 kcal/mol lower than the reactants. As discussed below, this product channel may be dominant at high temperature and low pressure. At low temperature and high pressure, the reaction should take place exclusively by the formation of $(C_6H_5)_2NO$ because of its large size and high stability.

Rate Constant Calculation. Rate constant calculations for the lowest energy paths by channels 1−3 have been performed in the temperature range 300−2000 K at pressures ranging from 10^{-3} Torr to 1000 atm. Helium was employed as buffer gas with their Lennard−Jones (L-J) parameters taken from the literature.[25] For the prediction of the quenching rates, the L-J parameters of the $(C_6H_5)_2NO$ radical were approximately estimated to be $\epsilon/k = 1004$ K and $\sigma = 3.56$ Å from the interaction potential between $(C_6H_5)_2NO$ and He, calculated at the B3LYP/6-31+G(d, p) level of theory. The averaged step-size for energy transfer per collision, $\langle\Delta E\rangle_{down}$, was taken to be 100 cm^{-1}.

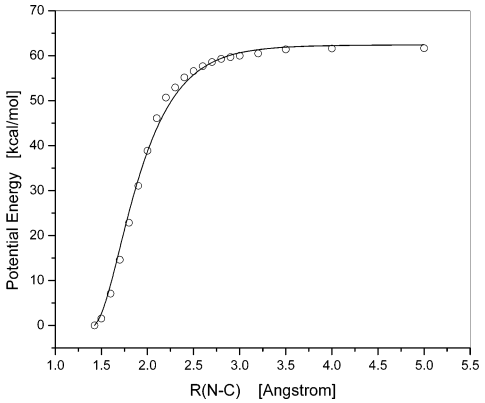

Figure 3. Potential energy curve for the dissociation process $(C_6H_5)_2NO \rightarrow C_6H_5NO + C_6H_5$. Points are computed at the B3LYP/6-31+G(d, p) level of theory, and solid curve is the fitted Morse function.

To carry out the variational transition-state rate calculation for the barrierless association process, $C_6H_5NO + C_6H_5 \rightarrow (C_6H_5)_2NO$, the minimum energy path was optimized by manually varying the separation of $C_6H_5N(O)\cdots C_6H_5$ point by point at an interval of 0.1 Å from $(C_6H_5)_2NO$ to the reactants at the B3LYP/6-31+G(d, p) level of theory, as shown in Figure 3. The association potential energy curve, which approximately represents their corresponding minimum energy path, can be fitted to the Morse function with the values of D_e and β, 61.7 kcal/mol and 2.71 $Å^{-1}$, respectively. Table 1 lists the moments of inertia and harmonic frequencies that were used to calculate rate constants for channels 1−3. As the small frequencies (such as 37 cm^{-1} for $(C_6H_5)_2NO$, 42 cm^{-1} for TS1, 26 cm^{-1} for TS7, and 10 cm^{-1} for TS8) correspond to internal rotations, we treated them simply as free rotators in the rate constant calculation.

Figure 4A shows the rate constants of channel 1 computed at 10^{-3}, 7, and 760 Torr and at the infinite pressure limit. In

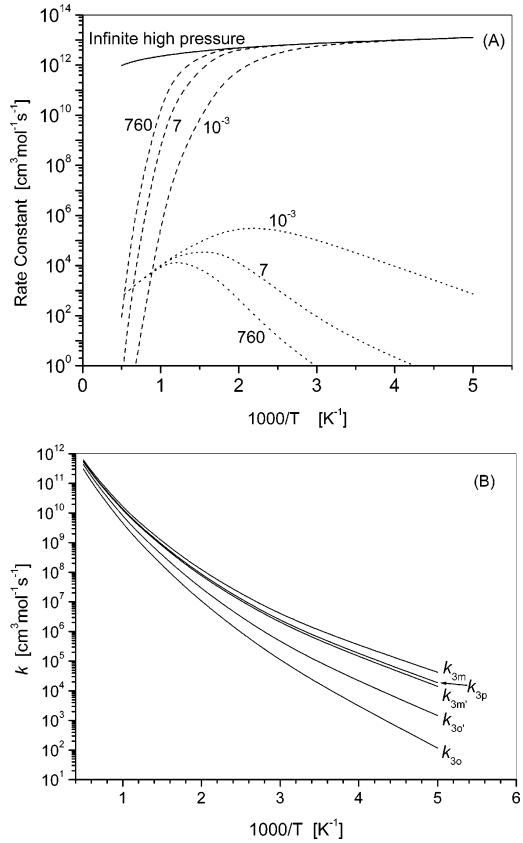

Figure 4. Predicted rate constants of channels 1 and 3. (A) products $(C_6H_5)_2NO$ (dashed lines) and P1 + H (dotted lines) at He pressures of 0.001, 7, and 760 Torr; (B) products $C_6H_4NO + C_6H_6$.

the figure, the solid line, dashed lines, and doted lines represent the values of k_1^{∞}, k_1[$(C_6H_5)_2NO$], and k_1(P1 + H), respectively. The rate constants for $(C_6H_5)_2NO$ formation can be fitted to the expressions:

$$k_1^{\infty} = 9.84 \times 10^{15}\, T^{-1.20} \exp(-58/T)\ [cm^3\, mol^{-1}\, s^{-1}] \quad (300-2000\ K)$$

$$k_{1,7\ Torr} = 6.83 \times 10^{17}\, T^{-1.85} \exp(-219/T)\ [cm^3\, mol^{-1}\, s^{-1}] \quad (300-500\ K)$$

$$= 2.57 \times 10^{177}\, T^{-52.08} \exp(-27984/T)\ [cm^3\, mol^{-1}\, s^{-1}] \quad (500-2000\ K)$$

$$k_1^0 = 4.68 \times 10^{38}\, T^{-5.48} \exp(-1316/T)\ [cm^6\, mol^{-2}\, s^{-1}] \quad (300-400\ K)$$

$$= 4.82 \times 10^{176}\, T^{-50.36} \exp(-21004/T)\ [cm^6\, mol^{-2}\, s^{-1}] \quad (400-2000\ K)$$

From Figure 4A, one sees that the high-pressure rate constant has a weak, negative temperature dependence. Its intermediate-pressure values depend strongly on pressure and exhibit strong negative temperature dependences in the high-temperature range. The rate constant for the formation of the P1 + H products, which is many orders of magnitude smaller than the association rate constant at 7 Torr preassure below 1000 K, have a positive temperature effect at low temperatures and a negative temperature effect at high temperatures. Due to competition with the stabilization of $(C_6H_5)_2NO$, the pressure effect for k_1(P1 + H) is negative. Also, we compare the rate constants of the P1 + H formation with and without multiple reflections above the LM1 well in the course of the $(C_6H_5)_2NO \rightarrow$ P1 + H reaction and found that the effect of multiple reflections is very small because this course is controlled primarily by TS2.

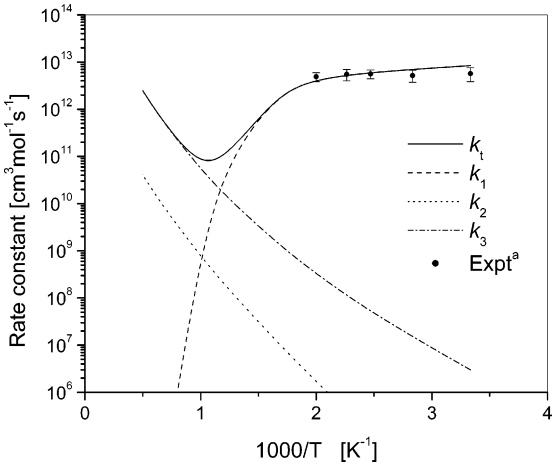

Figure 5. Comparison of the predicted rate constants with the experimental data. In this figure, $k_t = k_1 + k_2 + k_3$ and $k_3 = k_{3o} + k_{3o'} + k_{3m} + k_{3m'} + k_{3p}$. [a]Ref 3.

Figure 4B displays the rate constants of the five hydrogen abstraction reactions in channel 3. k_{3o}, $k_{3o'}$, k_{3m}, $k_{3m'}$, and k_{3p} represent the rate constants of these five processes through *o*-TS8, *o*′-TS8, *m*-TS8, *m*′-TS8, and *p*-TS8, respectively. The sum of these five rate constants is denoted as k_3, which is fitted to the expression:

$$k_3 = 3.21 \times 10^{-2}\, T^{4.34} \exp(-1953/T)\ [cm^3\, mol^{-1}\, s^{-1}] \quad (300-2000\ K)$$

The relative magnitudes of these rate constants are $k_{3m} > k_{3p} > k_{3m'} > k_{3o'} > k_{3o}$, reflecting primarily the steric hindrance effect of the NO group as alluded to before. Although these rate constants are small and negligible at lower temperatures, they become competitive at high temperatures.

Comparison of the theoretical rate constants with the experimental data reported by Park and Lin[3] is shown in Figure 5. The theoretical total rate constant (k_t) represents the sum of the three channel rate constants, $k_t = k_1 + k_2 + k_3$. From this figure, one can see that both k_2 and k_3 can be neglected at the temperatures below about 800 K. However, at higher temperatures, k_3 becomes dominant because of the strong negative temperature effect of k_1. Therefore, the major products of the $C_6H_5 + C_6H_5NO$ reaction system are predicted to be $(C_6H_5)_2NO$ at low temperatures and high pressures and $C_6H_4NO + C_6H_6$ at high temperatures and low pressures. Figure 5 clearly indicates that the major product formed in the experimental temperature range of 300−500 K at 7 Torr He pressure is $(C_6H_5)_2NO$, which is fully consistent with the experimental finding. The value of k_t at 7 Torr pressure can be given as follows:

$$k_{t,7\ Torr} = 3.94 \times 10^{21}\, T^{-3.09} \exp(-699/T)\ [cm^3\, mol^{-1}\, s^{-1}] \quad (300-500\ K)$$

$$= 2.09 \times 10^{20}\, T^{-3.56} \exp(2315/T)\ [cm^3\, mol^{-1}\, s^{-1}] \quad (500-1000\ K)$$

$$= 1.51 \times 10^{2}\, T^{3.30} \exp(-3043/T)\ [cm^3\, mol^{-1}\, s^{-1}] \quad (1000-2000\ K)$$

The product branching ratios based on the theoretical rate constants computed at 7 Torr are presented in Figure 6 as a

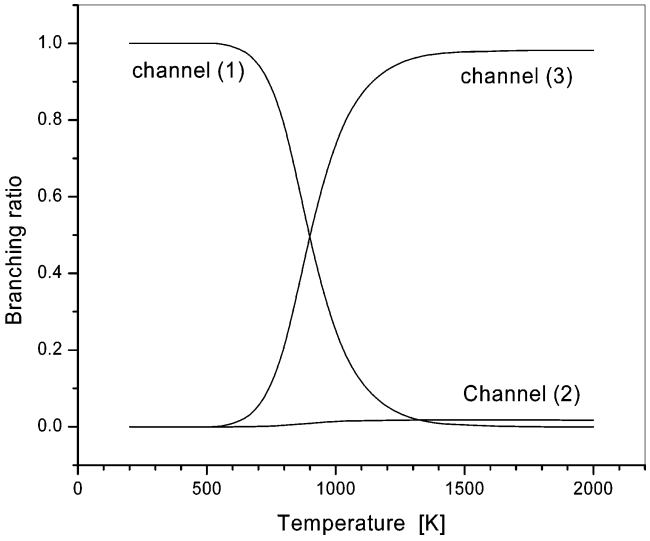

Figure 6. Theoretical branching ratios of three reaction channels relative to the total rate constant.

function of temperature. The result again illustrates the above conclusion that, at 7 Torr pressure at $T < 900$ K, the dominant reaction is channel 1; at $T > 900$ K the dominant reaction becomes channel 3 with contribution >90%. Channel 2 is too small to compete throughout the entire temperature range studied.

Conclusion

The mechanism of the $C_6H_5 + C_6H_5NO$ reaction has been studied at the B3LYP/6-31+G(d, p) level of theory. The result shows that the barrierless association producing $(C_6H_5)_2NO$ is dominant under the conditions studied in our previous experiment. In principle, the excited adduct can isomerize and decompose via the transition states with energies below the reactants producing H + N-hydroxyl carbazole at low pressures and higher temperatures. Hydrogen abstraction from C_6H_5NO by C_6H_5 can also take place via transition states with about 7 kcal/mol barriers at meta and para positions. These reactions may occur competitively above 900 K.

The rate constants have been predicted by the microcanonical RRKM and/or variational transition state theories in the temperature range of 300−2000 K. The total rate constant computed at 7 Torr He pressure can be given by $k_{t,7\ Torr} = 3.94 \times 10^{21} T^{-3.09} \exp(-699/T)$ for 300−500 K, which agrees reasonably with available experimental data within reported errors.

Acknowledgment. The authors are grateful for the support of this work from the Basic Energy Sciences, Department of Energy, under Contract DE-FG02-97-ER14784. We also thank the Cherry L. Emerson Center of Emory University for the use of its resources, which are in part supported by a National Science Foundation grant (CHE-0079627) and an IBM shared University Research Award. M.C.L. acknowledges the support from Taiwan National Science Council for a Distinguished Visiting Professorship at the Center for Interdisciplinary Molecular Science, Chiao Tung University, Hsinchu, Taiwan.

References and Notes

(1) Lin, C.-Y. Ph.D. Dissertation, Catholic University of America, Washington, DC, 1987.
(2) Wyatt, J. R.; Decorpo, J. J.; McDowell, W. V.; Saalfeld, F. E. *Rev. Sci. Instrum.* **1974**, *45*, 916.
(3) Park, J.; Lin, M. C. *J. Phys. Chem. A* **1997**, *101*, 14.
(4) Park, J.; Dyakov, I. V.; Lin, M. C. *J. Phys. Chem. A* **1997**, *101*, 8839.
(5) Park, J.; Gheyas, S. I.; Lin, M. C. *Int. J. Chem. Kinet.* **1999**, *31*, 645.
(6) Park, J.; Dyakov, I. V.; Mebel, A. M.; Lin, M. C. *J. Phys. Chem. A* **1997**, *101*, 6043.
(7) Yu, T.; Lin, M. C. *J. Am. Chem. Soc.* **1993**, *115*, 4371.
(8) Lin, M. C.; Yu, T. *Int. J. Chem. Kinet.* **1993**, *25*, 875. 9.
(9) Yu, T.; Lin, M. C. *J. Phys. Chem.* **1994**, *98*, 2105. 10.
(10) Yu, T.; Lin, M. C. *J. Am. Chem. Soc.* **1994**, *116*, 9571.
(11) Maschke, A.; Shapiro, B. S.; Lampe, F. W. *J. Am. Chem. Soc.* **1964**, *86*, 1929.
(12) Tan, H.-S.; Lampe, F. W. *J. Phys. Chem.* **1972**, *76*, 3303.
(13) (a) Gonzalez, C.; Schlegel, H. B. *J. Chem. Phys.* **1989**, *90*, 2154. (b) Gonzalez, C.; Schlegel, H. B. *J. Phys. Chem.* **1990**, *94*, 5523.
(14) (a) Becke, A. D.; *J. Chem. Phys.* **1993**, *98*, 5648. (b) Becke, A. D. *J. Chem. Phys.* **1992**, *96*, 2155.
(15) Lee, C.; Yang, W.; Parr, R. G. *Phys. Rev.* **1988**, *37B*, 785.
(16) Frisch, M. J.; Trucks, G. W.; Schlegel, H. B.; Scuseria, G. E.; Robb, M. A.; Cheeseman, J. R.; Zakrzewski, V. G.; Montgomery, J. A., Jr.; Stratmann, R. E.; Burant, J. C.; Dapprich, S.; Millam, J. M.; Daniels, A. D.; Kudin, K. N.; Strain, M. C.; Farkas, O.; Tomasi, J.; Barone, V.; Cossi, M.; Cammi, R.; Mennucci, B.; Pomelli, C.; Adamo, C.; Clifford, S.; Ochterski, J.; Petersson, G. A.; Ayala, P. Y.; Cui, Q.; Morokuma, K.; Malick, D. K.; Rabuck, A. D.; Raghavachari, K.; Foresman, J. B.; Cioslowski, J.; Ortiz, J. V.; Stefanov, B. B.; Liu, G.; Liashenko, A.; Piskorz, P.; Komaromi, I.; Gomperts, R.; Martin, R. L.; Fox, D. J.; Keith, T.; Al-Laham, M. A.; Peng, C. Y.; Nanayakkara, A.; Gonzalez, C.; Challacombe, M.; Gill, P. M. W.; Johnson, B. G.; Chen, W.; Wong, M. W.; Andres, J. L.; Head-Gordon, M.; Replogle, E. S.; Pople, J. A. *Gaussian 98*; Gaussian, Inc.: Pittsburgh, PA, 1998.
(17) (a) Wardlaw, D. M.; Marcus, R. A. *Chem. Phys. Lett.* **1984**, *110*, 230; *J. Chem. Phys.* **1985**, *83*, 3462. (b) Klippenstein, S. J. *J. Chem. Phys.* **1992**, *96*, 367. (c) Klippenstein, S. J.; Marcus, R. A. *J. Chem. Phys.* **1987**, *87*, 3410.
(18) Klippenstein, S. J.; Wagner, A. F.; Dunbar, R. C.; Wardlaw, D. M.; Robertson, S. H. *VARIFLEX*, version 1.00; 1999.
(19) Davico, G. E.; Bierbaum, V. M.; DePuy, C. H.; Ellison, G. B.; Squires, R. R. *J. Am. Chem. Soc.* **1995**, *117*, 2590.
(20) Choi, Y. M.; Lin, M. C. *Int. J. Chem. Kinet.* **2005**, *37*, 261.
(21) Wenthold, P. G.; Squires, R. R. *J. Am. Chem. Soc.* **1994**, *116*, 6401.
(22) Nam, G.-J.; Xia, W.; Park, J.; Lin, M. C. *J. Phys. Chem. A* **2000**, *104*, 1233.
(23) Chase, M. W., Jr.; Davles, C. A.; Downey, J. R., Jr.; Frurip, D. J.; McDonald, R. A.; Syverud, A. N. JANAF Thermochemical Tables. *J. Phys. Chem. Ref. Data* **1985**, *14* (Suppl. 1).
(24) Ruscic, B.; Feller, D.; Dixon, D. A.; Peterson, K. A.; Harding, L. B.; Asher, R. L.; Wagner, A. F. *J. Phys. Chem. A* **2001**, *105*, 1.
(25) Hippler, H.; Troe, J.; Wendelken, H. J. *J. Chem. Phys.* **1983**, *78*, 6709.